Int. J. Electrochem. Sci., 14 **(2019)** 9058 – 9068, doi: 10.20964/2019.09.76

International Journal of
ELECTROCHEMICAL
SCIENCE
www.electrochemsci.org

Electrodeposited Ni/phosphors Composite Coating for Latent Fingerprints Visualization

Xiaoshun Zhang[1,2], Kaiyue Zhang[1,2,3,], Wei Xiao[3], Jianguo Liu[3]*

[1] Criminal Investigation Police University of China, Shenyang 110035, China
[2] Key Laboratory of Impression Evidence Examination and Identification Technology, Ministry of Public Security, people 's republic of China, Shenyang 110035, China
[3] Institute of Metal Research, Chinese Academy of Sciences, Shenyang 110016, China
[*]E-mail: kyzhang@imr.ac.cn

Received: 11 May 2019 / *Accepted:* 1 July 2019 / *Published:* 5 August 2019

Fingerprint is a crucial means of physical evidence in forensic science owing to its uniqueness. It is important for identification to make those invisible latent fingerprints visible. Instead of methods based on making fingerprint secretions themselves visible, a novel approach involving electrochemically driven processes is proposed, through which fluorescent particles are innovatively introduced. The fingerprint secretions act as insulating masks, and then Ni/phosphors composite electrodeposition process only spatially selective occurs on bare metal surface between fingerprint ridges to generate a negative image of the fingerprint. In order to optimize the composite electrodeposition process, surfactant and concentration of phosphors in the electroplating solution are investigated. In addition, the fingerprint fluorescent visualization effects based on concentration of phosphors as well as electrochemical processing time are compared. The method presents the great advantage of being efficient, facile, and innoxious, particularly when the latent fingerprint is on a multicolored or dark background.

Keywords: latent fingerprint; forensic science; electrodeposition; phosphor; coating

1. INTRODUCTION

The fingerprint is extensively used as an important means of physical evidence in identification despite the increasingly use of other methods such as DNA-based tests [1]. It is the uniqueness of fingerprint that maintains the popularity of fingerprint evidence for forensic and other objectives. Specifically, fingerprint is unique to each person, can survive even in superficially damaged skin and remain unchanged during a person's lifetime. When one's finger touches an object, some secretions from fingertip are inevitably deposited on its surface to form fingerprints. Even though some circumstances such as paint and blood may result in visible fingerprint images, the majority of fingerprints left on objects are invisible, named as latent fingerprint.

Latent fingerprints include eccrine and sebaceous fingerprints, both of which need to enhance their visualization via a variety of chemical or physical treatments. The composition of secretions from fingertip is complex, including inorganic salt, amino acids, fatty acids, sterols and so on. Therefore, some reagents are firstly proposed to reveal latent fingerprint via chemically-based reaction with secretions, for example, ninhydrin [2-4], cyanoacrylate [5-8], physical developer [9] and so on. Besides, another conventional method for latent fingerprint visualization is to utilize powders which can be preferentially adhered to fingerprint secretions. Powders' fluorescent [10-14] as well as magnetic [15, 16] function are widely used to tender significant contrast with the background surface. Nevertheless, these traditional strategies have some obvious shortcomings, for example, inevitably damaging some fingerprint details, lower selectivity and contrast as well as higher toxicity [17]. In spite of great efforts being exerted for optimization, the success rate in obtaining high-quality fingerprints remains surprisingly low, especially for metal surfaces [18].

In recent years, rather than methods based on making fingerprint secretions themselves visible, a novel method involving electrochemical processes has been proposed. Specifically, fingerprint secretions, as insulating masks, make electrochemical processes only occur on trench regions of bare metal surface between fingerprint deposit ridges to form a negative image of the fingerprint. According to the strategy, some polymers were deposited to make latent fingerprint visible via electrochemical polymerization, such as polypyrrole [19], polyaniline [20], poly(3,4-ethylenediox-ythiophene) [21], Poly(Py-co-EDOT) [22] and so on. In addition, nano-sized Ag and Au also have been electrodeposited to generate visual contrast [23]. In this way, latent fingerprint can be effectively enhanced on many conductive surfaces regardless of whether they have enough fingerprint secretions or they are smooth. And the process is innoxious. Therefore, electrochemical methods for fingerprint visualization are very promising.

Herein, we report the complementary approach based on electrochemically driven processes, through which fluorescent particles are innovatively introduced. As shown in the Fig.1, the fingerprint secretions act as a template, and then Ni/phosphors composite electrodeposition process only spatially selective occurs on bare metal surface between fingerprint ridges to generate a negative image of the fingerprint. In order to optimize the enhancement process, surfactant and concentration of phosphors in the electroplating solution as well as the electrochemical processing time are investigated. The method presents the great advantage of being efficient, facile, and innoxious, particularly when the latent fingerprint is on a multicolored or dark background.

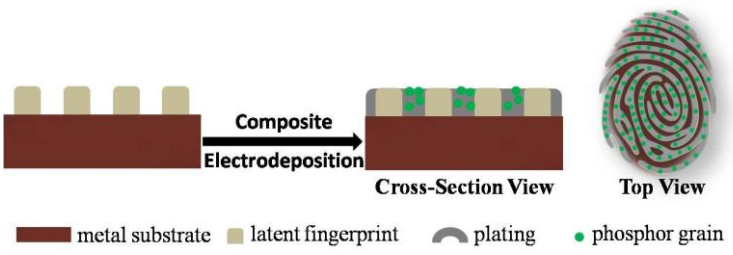

Figure 1. Schematic diagram of strategy for visualizing latent fingerprints via composite electrodeposition of Ni/phosphors.

2. EXPERIMENTAL

2.1 Substrates and Reagents

The copper foils (0.2 mm thickness) as the substrates were cut 20 mm×30 mm pieces, and ultrasonically cleaned in ethanol, then dried in air. $NiSO_4 \cdot 6H_2O$, $NiCl_2 \cdot 6H_2O$ and H_3BO_3 purchased from Sinopharm Chemical Reagent Co., Ltd. were used as received. Cetyltrimethyl Ammonium Bromide (CTAB), Sodium Dodecyl Sulfonate (SDS) and Octaphenyl Polyoxyethyiene-10 (OP-10) purchased from Tianjin Kermel Chemical Reagent Co., Ltd. were used as typical cationic, anionic and nonionic surfactant, respectively. The phosphors (chemical composition $SrAl_2O_4$: Eu) with particle sizes of 10 μm, 100 μm and 300 μm were purchased from Foshan XiuCai Chemicals Co., Ltd.

2.2 Latent fingerprints development

Before fingerprint deposition, the volunteer's hand should be thoroughly washed with liquid soap. Latent fingerprints were obtained via rubbing the volunteer's fingertip over the forehead and then touching the copper substrate lightly. Electrodeposition was carried out with an electrochemical workstation (Princeton Applied Research 273, USA) in a typical three-electrode cell with latent fingerprint sample (or copper foil) as the working electrode, Ag/AgCl reference electrode and platinum foil counter electrode. The basic electroplating solution contained 45 g/L $NiCl_2 \cdot 6H_2O$ and 300 g/L $NiSO_4 \cdot 6H_2O$. Commercial phosphors were added into the electroplating solution to prepare the composite electroplating solutions with different phosphors concentrations (10 $g \cdot L^{-1}$, 20 $g \cdot L^{-1}$, 30 $g \cdot L^{-1}$, 40 $g \cdot L^{-1}$, 50 $g \cdot L^{-1}$). 38 $g \cdot L^{-1}$ H_3BO_3 was studied to enhance the stability of phosphors in composite electroplating solutions. In addition, CTAB, SDS and OP-10 three typical surfactants with different content ranging from 0.1 $g \cdot L^{-1}$ to 0.9 $g \cdot L^{-1}$ were added to investigate the improvement for phosphors content in the composite coatings. During the electrodeposition process, the cathodic current density was controlled at 30 $mA \cdot cm^{-2}$ according to our previous work experience (The corresponding electrode potential was about -0.65 V vs. RHE). The magnetic stirring (250 rpm) ensured the suspension state of phosphors in the composite electroplating solution and the operating temperature was 45 °C. After electrodeposition, the samples were washed with deionized water and dried in air.

2.3 Characterization methods

365 nm UV radiation was provided by TY-365nm-3w UV flashlight (Shenzhen TaoYuan Co., Ltd.). Canon EOS 6D digital camera was utilized to obtain fingerprint images. The crystalline structure of phosphors was characterized by XRD (Rigaku, D/Max-2400). The surface morphology of Ni/phosphors composite coatings was observed by SEM (JEOL, JSM-6300), and the phosphors content in the composite coating was measured by EDS (JEOL, JSM-6300).

3. RESULTS AND DISCUSSION

The solid luminescent materials as one of the important functional materials have attracted more and more attention, particularly for long afterglow luminescent phosphors. According to their host material, long afterglow phosphors can be divided into three classifications: aluminates, sulphides and silicates, among which aluminates have wide application prospects because of their longer afterglow time as well as higher brightness. Therefore, we employ aluminates phosphors to provide fluorescence function in this work. As shown in Fig.2A, the fluorescent brightness increases with the particle size enlarging. They all generate yellow-green light, but the brightness of 300 μm particles is much stronger than that of 10 μm particles. Even though the bigger one has a brighter fluorescent brightness, it is difficult for large size particles to be co-deposited with metal ions. According to previous researches [24-27], micro-nano sized particles (500 nm - 50 μm) are the ideal size to be used to co-deposition. Specifically, smaller particles (< 500 nm) tend to agglomerate and agglomerate, which hinders their migration to the cathode and reduces their content in the coating. Meanwhile, bigger particles (> 50 μm) have poor suspension properties and are less likely to diffuse to the surface of the cathode. For fingerprint visualization, the selection of the phosphors should be based on the coordination between fluorescent brightness and co-deposition feasibility. Accordingly, commercial 10 μm aluminates phosphors (Fig.2B) are used in the work, which have enough fluorescent brightness as well as proper particle size.

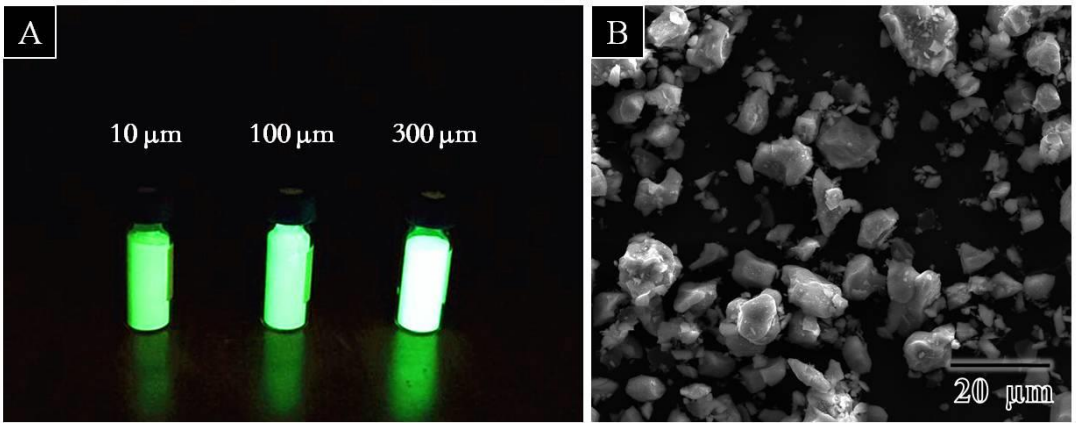

Figure 2. (A) The fluorescent brightness contrast of 10 μm, 100 μm and 300 μm phosphors particles and (B) SEM image of 10 μm phosphors particles.

As is well known, the aluminates are easy to hydrolyze, which not only shorten their working life but also may affect the stability of the composite electroplating solution. In order to overcome the shortcoming, H_3BO_3 as stabilizer and pH buffer is studied to improve the stability of phosphors in the composite electroplating solution. Fig.3A shows the fluorescent brightness contrast of the composite electroplating solution without H_3BO_3 before and after 5d. It can be clearly observed that the electroplating solution after 5d nearly has no fluorescent brightness, in which the phosphors have become white colour. According to the XRD data (Fig.3D blue line), the white products have some

sharp diffraction peaks belonging to $Sr_3Al_2(OH)_{12}$ (JCPDS: 24-1186), such as (211), (321), (420), (521) and (611). However, the pristine phosphors (Fig.3D black line) show entirely different diffraction peaks belonging to $SrAl_2O_4$ (JCPDS: 34-0379). The white products are typical hydrolysis products of aluminates without any fluorescence, which proves that phosphors can not stably exist in the electroplating solution without H_3BO_3. As is expected, the fluorescent brightness of the composite electroplating solution with H_3BO_3 (Fig.3B) almost remains unchanged as a function of time, and the phosphors do not change their colour and still show main diffraction peaks of $SrAl_2O_4$, such as (011), (-211) and (031) (Fig.3D red line). In order to analyze the role of H_3BO_3 for stabilization function in the composite electroplating solution, H_3BO_3 solution is prepared and fluorescent brightness of phosphors in H_3BO_3 solution is studied as shown in Fig.3C.

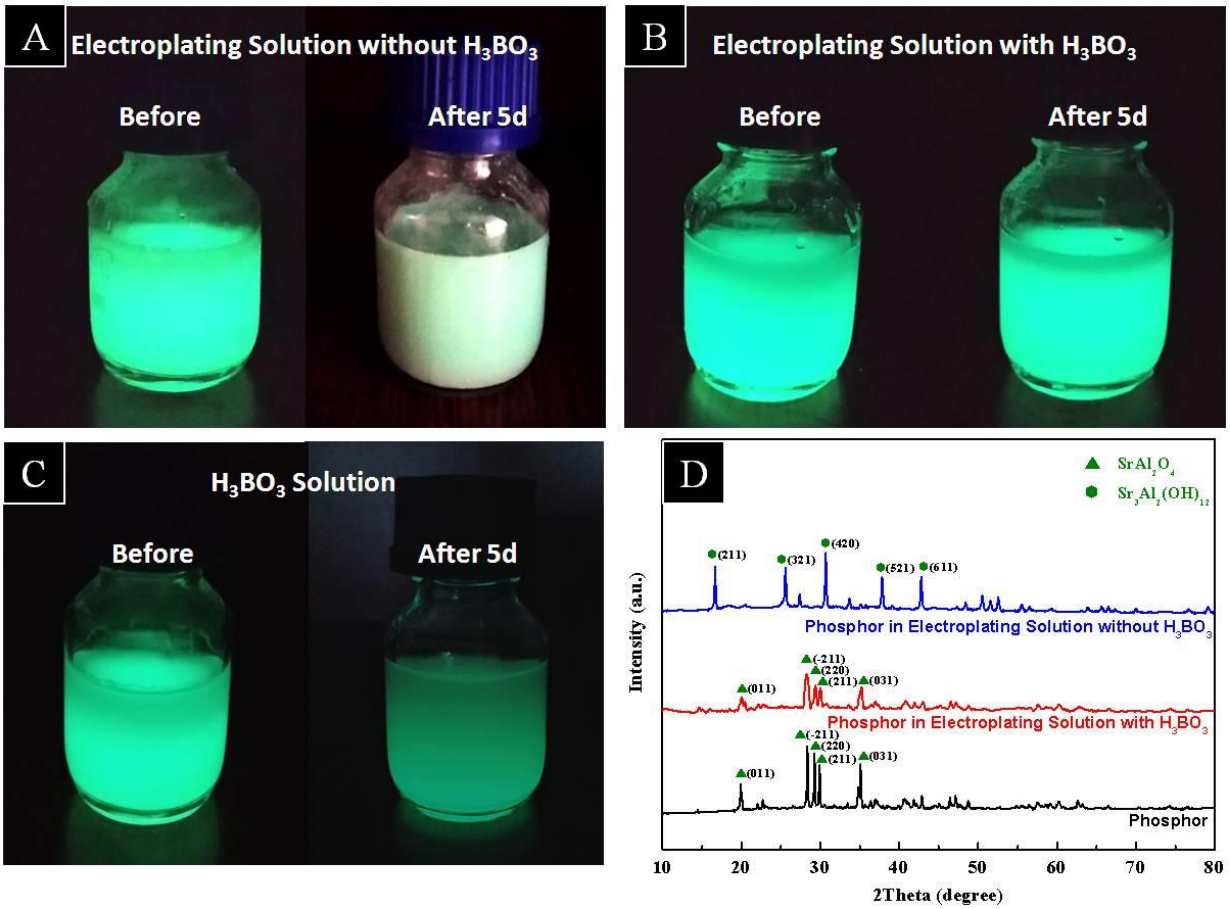

Figure 3. The fluorescent brightness contrast of the composite electroplating solution containing 40 $g \cdot L^{-1}$ phosphors before and after 5d (A) without H_3BO_3 and (B) with 38 $g \cdot L^{-1}$ H_3BO_3; (C) The fluorescent brightness contrast of 38 $g \cdot L^{-1}$ H_3BO_3 aqueous solution containing 40 $g \cdot L^{-1}$ phosphors before and after 5d; (D) The XRD of pristine phosphors, phosphors after 5d in electroplating solution without and with H_3BO_3.

As we can see, the fluorescent brightness obviously declines after 5d, which indicates that a part of phosphors hydrolyze in the H_3BO_3 solution. Therefore, the hydrolysis reaction of phosphors cannot be completely inhibited only depending on H_3BO_3, and the hydrolysis inhibition may result from the synergistic effect of H_3BO_3 and Ni^{2+} solution as proved in Fig.3B. Specifically, H_3BO_3 as a

weak acid and Ni^{2+} as the conjugate base jointly constitute a buffer system to inhibit hydrolysis of added phosphors to a certain degree. In conclusion, H_3BO_3 serves as the premise for a stable composite electroplating solution and may cooperate with the main salt (Ni^{2+}) to ensure chemical stabilization of phosphors.

In order to preferably visualize latent fingerprint, enough phosphors should be co-deposited in the trench regions of bare metal surface between fingerprint deposit ridges. The surfactants can improve the suspension and charge property of particles in the composite solutions, which will contribute to the co-deposition content of particles in the composite coating. Fig.4 shows the co-deposited phosphors content changes in the composite coating with the increasing of the concentration of three typical surfactants in the electroplating solution. For CTAB (cationic surfactant), its existence can increase the co-deposition content of phosphors, which is in accordance with the previous work [28]. The co-deposition content sharply increases with the concentration of CTAB in the electroplating solution increasing at lower concentrations, the reason of which is that the increase of positive charges absorbed on phosphors accelerates the movement of the phosphors towards the negative working electrode and thus increase the co-deposition content. After reaching the maximum (13.5 wt. %), the co-deposition content gradually declines with the concentration of CTAB increasing, which can be ascribed to the repulsive interaction between the positive phosphors and the excessive inevitable positive charges absorbed on the working electrode. Compared with CTAB, SDS (anionic surfactant) has a negative influence on the co-deposition content of phosphors. The co-deposition content gradually declines with the concentration of SDS increasing. The result can be explained by the work [29] that negative charges absorbed on phosphors hinder the migration of phosphors to the cathode. That is, like charge repulsion between the negative working electrode and negative phosphors hinders the co-deposition. Additionally, for OP-10 (nonionic surfactant), it has a little positive influence on the co-deposition content of phosphors. Since OP-10 can increase intermolecular force, the suspension property of phosphors in the electroplating solution is improved and thus increases the co-deposition content of phosphors. From what has been discussed above, the proper cationic surfactant can improve the co-deposition content of phosphors.

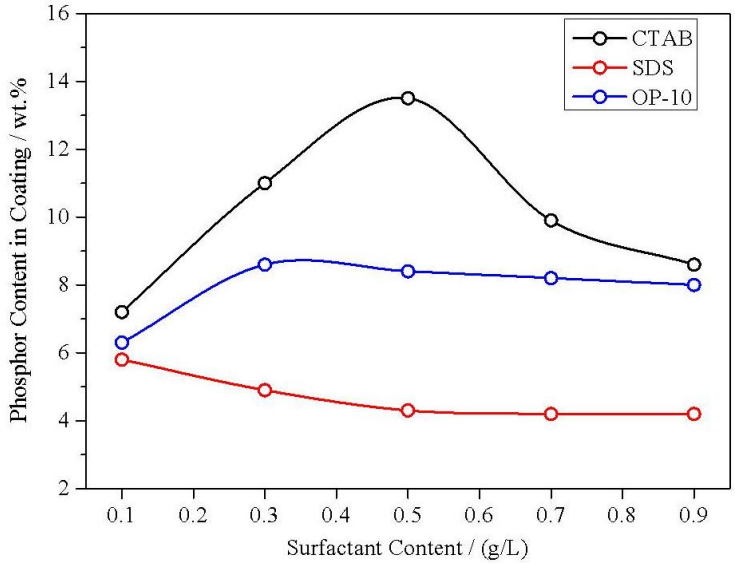

Figure 4. The co-deposited phosphors content change in the composite coating with the increasing of the concentration of CTAB (black line), SDS (red line) and OP-10 (blue line) in the composite electroplating solution (45 $g \cdot L^{-1}$ $NiCl_2 \cdot 6H_2O$, 300 $g \cdot L^{-1}$ $NiSO_4 \cdot 6H_2O$, 38 $g \cdot L^{-1}$ H_3BO_3 and 40 $g \cdot L^{-1}$ phosphors). The electrodeposition time is 200 s.

The concentration of phosphors in the composite electroplating solution likewise plays an important role in improving the co-deposition. A series of composite coatings deposited in the composite electroplating solution with different concentration of phosphors are prepared. The SEM images of the composite coatings are compared in Fig. 5A-E. The co-deposited phosphors distribution in the composite coatings is found to be intensive with a rise in the concentration of phosphors when the concentration increases ranging from 10 $g \cdot L^{-1}$ to 40 $g \cdot L^{-1}$. And the distribution also becomes increasingly uniform. The above phenomenon may be attributed to the fact that the increase in concentration of phosphors results in a higher chance of collision to the working electrode. However, once the concentration is too high (Fig. 5E), more intense collision among phosphors can influence the co-deposition. The bigger particles are hardly co-deposited on the composite coating and the distribution becomes sparse. It is worth mentioning, the co-deposited phosphors are embedded in the Ni matrix as shown in Fig. 5F, which ensures the adhesion resistance of co-deposited phosphors in the composite coating. The corresponding co-deposited phosphors content with different concentrations of phosphors is shown in Fig. 6. The co-deposited phosphors content radically increases with the concentration of phosphors increasing when the concentration is lower than 40 $g \cdot L^{-1}$, which is in accordance with SEM results and some previous works [30-31]. The higher concentration of the particles in the electroplating solution, that is, the more particles transported to the cathode surface via stirring can result in a greater probability that the particles are co-deposited in the composite coating. Not surprisingly, the co-deposited phosphors content decreases when the concentration increases to 50 $g \cdot L^{-1}$ due to extremely high concentration of phosphors. The similar results have been proven in the previous works [32-33]. Therefore, 40 $g \cdot L^{-1}$ phosphors are ideal concentration to obtain optimal phosphors distribution and content in the composite coating.

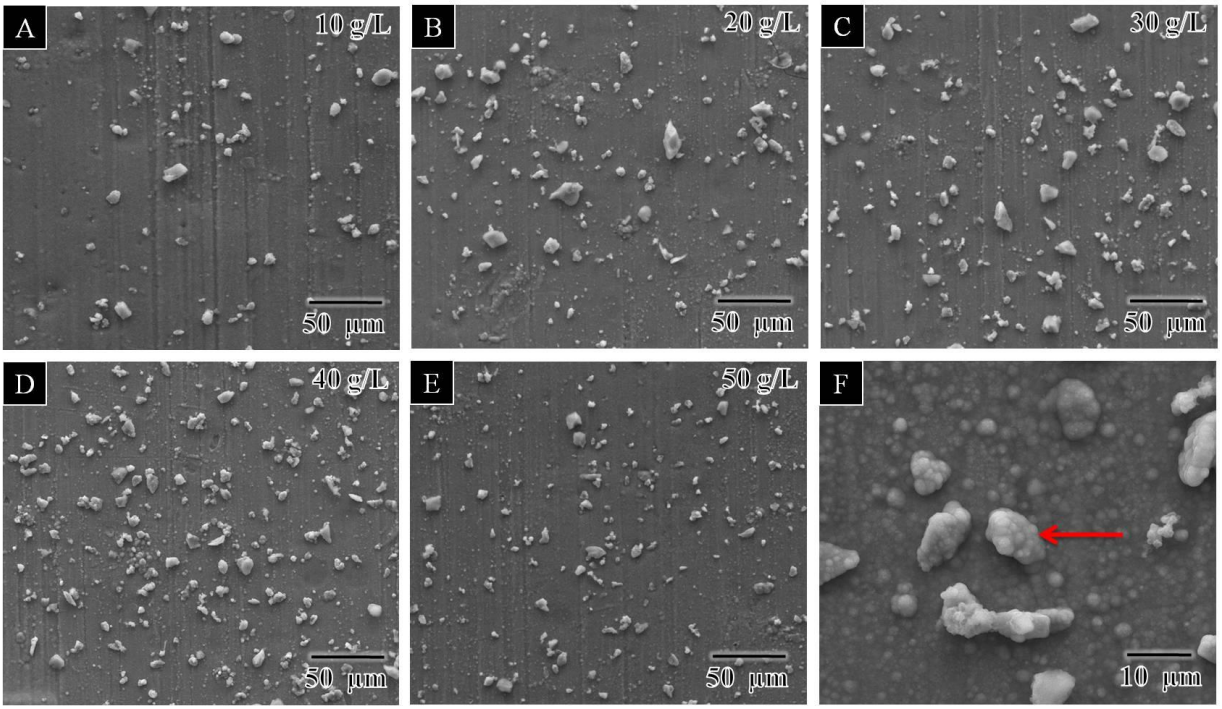

Figure 5. SEM images of the composite Ni/phosphors coatings deposited in the composite electroplating solution with (A) 10 $g \cdot L^{-1}$ phosphors; (B) 20 $g \cdot L^{-1}$ phosphors; (C) 30 $g \cdot L^{-1}$ phosphors; (D) 40 $g \cdot L^{-1}$ phosphors; (E) 50 $g \cdot L^{-1}$ phosphors. The composite electroplating solution contains 45 $g \cdot L^{-1}$ $NiCl_2 \cdot 6H_2O$, 300 $g \cdot L^{-1}$ $NiSO_4 \cdot 6H_2O$, 38 $g \cdot L^{-1}$ H_3BO_3 and 0.5 $g \cdot L^{-1}$ CTAB. And the electrodeposition time is 200 s. (F) SEM image of co-deposited phosphors.

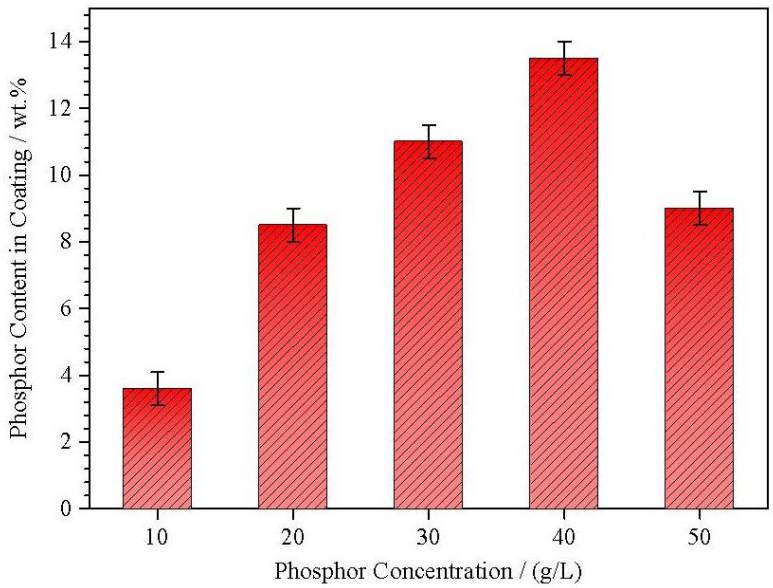

Figure 6. The corresponding co-deposited phosphors content in the composite coating with different concentrations of phosphors in the electroplating solution.

Subsequently, the fingerprint fluorescent visualization effects with different concentrations of phosphors are compared in Fig.7. The sample with 10 $g \cdot L^{-1}$ phosphors (Fig. 7A) only produces a weak contrast between the ridges and the trenches, and details of the fingerprint could not be visualized clearly. As the concentration of phosphors increasing (Fig. 7B-D), the fingerprint fluorescent visualization effects get much improved due to more phosphors co-deposited on the bare metal surface between fingerprint deposit ridges as proved above. The sample with 40 $g \cdot L^{-1}$ phosphors (Fig. 7D) shows the highest contrast fingerprint details such as ridge endings and bifurcations which are important for the identification of fingerprints.

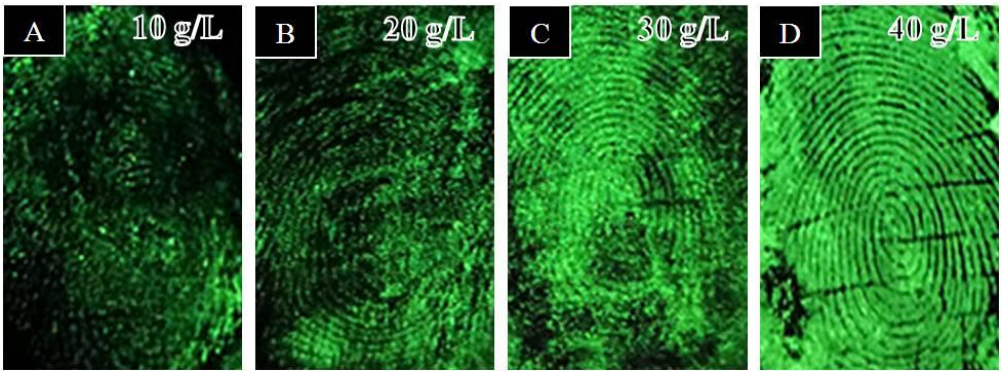

Figure 7. Latent fingerprints enhanced by electrodeposition of Ni/phosphors coatings deposited in the composite electroplating solution with different concentrations of phosphors (A: 10 $g \cdot L^{-1}$ phosphors; B: 20 $g \cdot L^{-1}$ phosphors; C: 30 $g \cdot L^{-1}$ phosphors; D: 40 $g \cdot L^{-1}$ phosphors). The electrodeposition time is 200 s.

The electrodeposition time is finally optimized for producing high-quality fingerprint. Fig.8 shows the fingerprint fluorescent visualization effects with different deposition time. When the deposition time is shorter (Fig.8A), only a part of latent fingerprints are visualized, which results from the fact that the trenches are not adequately co-deposited by the Ni/phosphors coating. As the deposition time increasing to 200 s, the high contrast fingerprint is clearly visualized as shown in Fig.8B (or Fig.7D). However, deposition time extending to 250 s (Fig.8C) results in worse contrast due to the consequence of the Ni/phosphors coating overfilling to the fingerprint ridges. In the previous work about visualization of latent fingerprints via prussian blue thin films [34], a similar result has been obtained that only under a optimal process time can a high contrast fingerprint be clearly visualized. In conclusion, the sample with 200 s electrodeposition time shows continuous composite coating within the trenches and clear definition at the ridge edges.

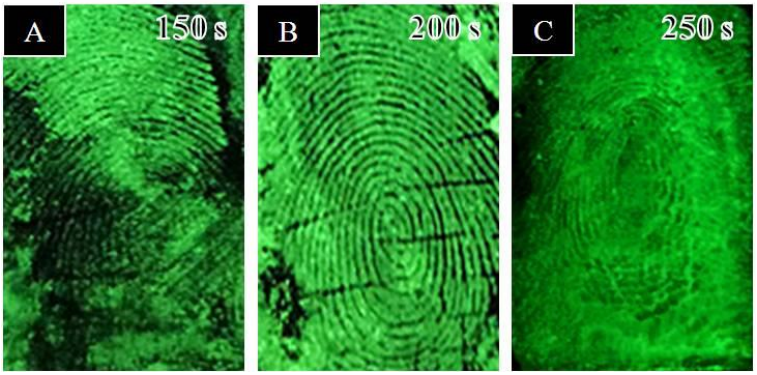

Figure 8. Latent fingerprints enhanced by electrodeposition of Ni/phosphors coatings with different operating time (A: 150 s; B: 200 s; C: 250 s). The concentration of phosphors is 40 $g \cdot L^{-1}$.

4. CONCLUSION

In the paper, a novel latent fingerprint visualization method involving electrochemically driven processes is proposed, through which fluorescent particles are innovatively introduced. The fingerprint secretions act as insulating masks, and then Ni/phosphors composite electrodeposition process only spatially selective occurs on bare metal surface between fingerprint ridges to generate a negative image of the fingerprint. In order to obtain a stable composite electroplating solution, H_3BO_3 is added and the hydrolysis inhibition may result from the synergistic effect of H_3BO_3 and Ni^{2+} solution. The proper cationic surfactant can improve the co-deposition content of phosphors. And 40 $g \cdot L^{-1}$ phosphors are ideal concentration to obtain optimal phosphors distribution and co-deposition content in the composite coating. As the deposition time increasing to 200 s, the high contrast fingerprint details are clearly visualized, such as ridge endings and bifurcations.

CONFLICTS OF INTEREST
There are no conflicts to declare.

ACKNOWLEDGEMENTS
The authors would like to acknowledge the support of the Ministry of Public Security Science and Technology Special Project (2017GABJC10), Key Laboratory of Impression Evidence Examination and Identification Technology, Ministry of Public Security, People's Republic of China (2018HJKF10), National Natural Science Foundation of China (No. 21676282) and Shenyang Science and Technology Project (No. 18013051).

References

1. H.C. Lee, R.E. Gaensslen, *Advances in Fingerprint Technology, CRC Press*, (2001) Boca Raton, USA.
2. J. Almog, V. G. Sears, E. Springer, D.F. Hewlett, S. Walker, S. Wiesner, R. Lidor, E. Bahar, *J. Forensic Sci.,* 45 (2000) 538.
3. R. Jelly, E. L. T. Patton, C. Lennard, S.W. Lewis, K.F. Lim, *Anal. Chim. Acta*., 652 (2009) 128.
4. H. Kobus, P. Pigou, S. Jahangiri, B. Taylor, *J. Forensic Sci*., 47 (2002) 254.
5. M. Colella, A. Parkinson, T. Evans, C. Lennard, C. Roux, *J. Forensic Sci*., 54 (2009) 583.

6. P. Czekanski, M. Fasola, J. Allison, *J. Forensic Sci*., 51 (2006) 1323.
7. S. Chadwick, P. Maynard, P. Kirkbride, C. Lennard, X. Spindler, C. Roux, *J. Forensic Sci*., 56 (2011) 1505.
8. C. Prete, L. Galmiche, F.G. Quenum-Possy-Berry, C. Allain, N. Thiburce, T. Colard, *Forensic Sci. Int*., 233 (2013) 104.
9. A. A. Cantu, *Forensic Sci. Rev*. 13 (2001) 32.
10. N. Akiba, N. Saitoh, K. Kuroki, *J. Forensic Sci*., 52 (2014) 1103.
11. M. Wang, M. Li, A. Y. Yu, J. Wu, C. B. Mao, *ACS Appl. Mater. Interfaces*, 7 (2015) 28810.
12. K. Cai, R. Yang, Y. Wang, X. Yu, J. Liu, *Forensic Sci. Int*., 226 (2013) 240.
13. M. Algarra, K. Radotić, A. Kalauzi, D. Mutavdžić, A. Savić, J. Jiménez-Jiménez, E. Rodríguez-Castellón, J.C. da Silva, J.J. Guerrero-González, *Anal. Chim. Acta*, 812 (2014) 228.
14. M. Algarra, D. Bartolić, K. Radotić, D. Mutavdžić, M.S. Pino-Gonzalez, E. Rodríguez-Castellón, J. Martínez, J.J. Guerrero-González, J.C. da Silva, J. Jiménez-Jiménez, *Talanta*, 194 (2019) 150.
15. L.K. Seah, U.S. Dinish, W.F. Phang, Z.X. Chao, V.M. Murukeshan, *Forensic Sci. Int*., 152 (2005) 249.
16. A.M. Boddis, D.A. Russell, *Anal. Methods*, 4 (2012) 637.
17. M. Wang, M. Li, A. Yu, Y. Zhu, M. Yang, C. Mao, *Adv. Funct. Mater*., 27 (2017) 1606243.
18. S.P. Wargacki, L.A. Lewis, M.D. Dadmun, *J. Forensic Sci.*, 53 (2008) 1138.
19. C. Bersellini, L. Garofano, M. Giannetto, F. Lusardi, G. Mori, *J. Forensic Sci.,* 46 (2001) 871.
20. A. L. Beresford, A.R. Hillman, *Anal. Chem*., 82 (2010) 483.
21. R.M. Brown, A.R. Hillman, *Phys. Chem. Chem. Phys*., 14 (2012) 8653.
22. R.M. Sapstead, N. Corden, A.R. Hillman, *Electrochim. Acta*, 162 (2015) 119.
23. G. Qin, M. Zhang, Y. Zhang, Y. Zhu, S. Liu, W. Wu, X. Zhang, *J. Electroanal. Chem*., 693 (2013) 122.
24. K. Zhang, J. Li, W. Liu, J. Liu, C. Yan, *Int. J. Hydrogen Energy*, 41 (2016) 22643.
25. B. Xu, H. Wang, S. Dong, B. Jiang, W. Tu, *Electrochem. Commun*., 7 (2005) 572.
26. I. Garcia, J. Fransaer, J.P. Celis, *Surf. Coat. Tech*., 148 (2001) 171.
27. H.K. Lee, H.Y. Lee, J.M. Jeon, *Surf. Coat. Tech*., 201 (2007) 4711.
28. E. Rudnik, L. Burzynska, Ł. Dolasiński, M. Misiak, *Appl. Surf. Sci.*, 256 (2010) 7414.
29. G. Yasin, M. Arifa, M.N. Nizama, M. Shakeela, M.A. Khanc, W.Q. Khand, T.M. Hassane, Z. Abbasa, I. Farahbakhsh, Y. Zuo, *RSC Adv.*, 8 (2018) 20039.
30. I. Haq, T. Khan, *Surf. Coat. Tech.*, 205 (2011) 2871.
31. A. Robin, J.L. Rosa, M.B. Silva, *Surf. Coat. Tech.*, 205 (2010) 2152.
32. W. Chen, W. Gao, *Electrochim. Acta*, 55 (2010) 6865.
33. Y. Yang, F.Y. Chen, *Surf. Coat. Tech.*, 205 (2010) 3198.
34. G. Qin, M. Zhang, Y. Zhang, Y. Zhu, S. Liu, W. Wu, X. Zhang, *Chinese Chem. Lett.*, 24 (2013) 173.